Numerical study of multisoliton configurations in a doped antiferromagnetic Mott insulator

Mona Berciu and Sajeev John
Department of Physics, University of Toronto, 60 St. George Street, Toronto, Ontario, Canada M5S 1A7
(Received 18 May 1998; revised manuscript received 26 February 1999)

We evaluate from first principles the self-consistent Hartree-Fock energies for multisoliton configurations in a doped, spin-$\frac{1}{2}$, antiferromagnetic Mott insulator on a two-dimensional square lattice. The microscopic Hamiltonian for this system involves a nearest-neighbor electron hopping matrix element t, an on-site Coulomb repulsion U, and a nearest-neighbor Coulomb repulsion V. We find that nearest-neighbor Coulomb repulsion on the energy scale of t stabilizes a regime of charged meron-antimeron vortex soliton pairs over a region of doping from $\delta=0.05$ to 0.4 holes per site for intermediate coupling $3\leqslant U/t\leqslant 8$. This stabilization is mediated through the generation of ''spin flux'' in the mean-field antiferromagnetic (AFM) background. Spin flux is a form of spontaneous symmetry breaking in a strongly correlated electron system in which the Hamiltonian acquires a term with the symmetry of spin-orbit coupling at the mean-field level. Spin flux modifies the single quasiparticle dispersion relations from that of a conventional AFM. The modified dispersion is consistent with angle-resolved photoemission studies and has a local minimum at wave vector $\vec{k}=\pi/2a(1,1)$, where a is the lattice constant. Holes cloaked by a meron vortex in the spin-flux AFM background are charged bosons. Our static Hartree-Fock calculations provide an upper bound on the energy of a finite density of charged vortices. This upper bound is lower than the energy of the corresponding charged spin-polaron configurations. A finite density of charge carrying vortices is shown to produce a large number of unoccupied electronic levels in the Mott-Hubbard charge transfer gap. These levels lead to significant band tailing and a broad midinfrared band in the optical absorption spectrum as observed experimentally. In the presence of a finite density of charged meron-antimeron pairs, the peak in the magnetic structure at $\vec{Q}=\pi/a(1,1)$, corresponding to the undoped AFM, splits into four satellite peaks that evolve with charge carrier concentration as observed experimentally. At very low doping ($\delta<0.05$) the doping charges create extremely tightly bound meron-antimeron pairs or even isolated conventional spin polarons, whereas for very high doping ($\delta>0.4$) the spin background itself becomes unstable to formation of a conventional Fermi liquid and the spin-flux mean field is energetically unfavorable. Our results point to the predominance of a quantum liquid of charged, bosonic, vortex solitons at intermediate coupling and intermediate doping concentrations. [S0163-1829(99)06923-4]

I. INTRODUCTION

A microscopic description of doped, spin-$\frac{1}{2}$, Mott insulators[1,2] is a central issue in the understanding of strongly correlated electrons and high-temperature superconductivity.[3] Of particular interest is the intermediate doping regime of $\delta=0.05-0.30$ charge carriers per lattice site on a two-dimensional square lattice. In this regime it has been observed, in a variety of cuprate superconducting materials, that long-range antiferromagnetic (AFM) order is destroyed by the presence of charge carriers and that these charge carriers lead to a variety of non-Fermi-liquid characteristics in the transport and electromagnetic response. The electrical,[4] magnetic,[5] and optical properties[6] of the doped parent compound, from which superconductivity emerges, are among the most glaring and profound mysteries in solid state physics today.[7,8]

In most theoretical studies of the doped Mott insulator, it has been assumed that the Coulomb repulsion between electrons can be described by a Hubbard model in which this interaction is replaced by a pointlike on-site interaction. Moreover, it has been assumed that the on-site Hubbard parameter U is an order of magnitude larger than the nearest-neighbor electron hopping energy scale t. This picture is based on the Fermi-liquid theory notion of screening of the effective electron-electron interaction. However, it is this same Fermi-liquid picture that studies of the Hubbard model seek to supplant. In some recent papers[9–12] we have shown that the nearest-neighbor Coulomb interaction is a highly relevant perturbation that can lead to an entirely different type of broken symmetry in the many-electron system. At the mean-field level we showed that Coulomb effects may give rise to a mean-field (Hartree-Fock) state in which the Hamiltonian acquires a term with the symmetry of a spin-orbit interaction. In this state, which we refer to as a spin-flux phase, the internal wave function of the electron (in spin space) undergoes a 2π rotation as the electron encircles any elementary plaquette of the two-dimensional (2D) square lattice. It was shown that spin flux itself is a dynamical variable that appears in quantized units and is carried by neutral skyrmion textures even within the undoped AFM. It was shown[10] that in the presence of a mean field of such spin flux, the mean-field ground-state energy is lower than in the absence of the spin flux (i.e., in the conventional AFM phase) for a large range of doping concentrations and on-site repulsion strength U.

These early comparisons of the spin-flux states with non-spin-flux states[10] assumed that the doping electrons (holes) formed extended states within the Mott-Hubbard bands lead-

 ©1999 The American Physical Society

ing to a global twist of the AFM background into a single wave-vector, incommensurate spiral state. More recently we have shown that the added charge carriers find it energetically favorable, in the majority of cases, to nucleate a point defect in the AFM background (charged magnetic soliton) rather than occupy a band state.[11,12] The existence of these charged solitons provides a remarkable and clear microscopic mechanism for non-Fermi-liquid behavior in a doped Mott insulator. Starting from the microscopic many-electron Hamiltonian, we derived a simple continuum model for the description of the magnetic soliton textures, such as skyrmions and merons, which are generated by doping of the antiferromagnetic parent compound. This continuum model recaptures the Mott-Hubbard gap structure by retaining the exact electron dynamics and AFM spin correlations on the scale of the elementary lattice plaquette. It is approximate in the sense that it assumes that the local magnetic structure varies slowly from one plaquette to the next and that the electron dispersion relations are linearized about the relevant Fermi points. The existence of magnetic textures leads to the appearance of bound levels deep inside the Mott-Hubbard charge-transfer gap. A doping hole can considerably lower its energy by occupying such a bound level, with the effect that the hole becomes trapped in the core of the magnetic soliton, in turn stabilizing the soliton. This leads to a striking analogy between the 2D AFM and the 1D polyacetylene.[13] In both cases, the mean-field ground state of the undoped system is degenerate as a result of broken symmetry. In both cases, doping induces topological fluctuations (solitons) that tend to restore the broken symmetry. In particular, we have shown that skyrmions (magnetic spin polarons) are the 2D analogs of 1D polarons in polyacetylene, while charged meron vortices are the 2D analogs of the charged bosonic domain-wall solitons in polyacetylene.[14] At the topological level a polaron in one dimension can be thought of as a tightly bound pair of domain walls, whereas a skyrmion in two dimensions is topologically equivalent to a bound meron-antimeron pair.[15] The analogy also holds at the level of the electronic structure. Both the 1D domain wall in polyacetylene and the 2D charged meron vortex in the AFM lead to the occurrence of mid-gap electron states in their respective one-electron band structures. It is well known that in polyacetylene, the first charge carrier added to the undoped polymer creates a polaron around itself, while a second charge carrier causes this polaron to split into two independent domain walls, each carrying one dopant. We suggested[12] that a similar picture holds in the 2D AFM: The first hole is cloaked by a magnetic spin polaron, while a second hole causes the polaron to split into a bound meron-antimeron pair, each vortex carrying a doping charge.

Neutral vortex-antivortex bound pairs may appear without doping in the layered AFM parent compound as the temperature is increased.[16] At finite doping, similar charged pairs appear even at $T=0$ since the increase in energy due to the distortion in the AFM background is compensated for by the energy gained through trapping the holes in midgap states near the vortex cores. If the doping reaches a critical value, these pairs may unbind even at $T=0$, leading to the destruction of long-range AFM order. For dopings smaller than this critical doping, a finite temperature may also entropically drive the transition from the AFM ordered state to a disordered ''spin liquid.''

In this article we treat the $T=0$ case and demonstrate that a transition from a dilute gas of charged spin polarons to a liquid of charged meron-vortex solitons takes place for intermediate doping and for intermediate values of U/t in the Hartree-Fock picture. The meron vortices are bosonic charge carriers, with deep electronic gap levels localized in their cores. The bosonic character may provide an explanation for the unusual non-Fermi-liquid properties of the metal observed in the intermediate doping region, while the deep gap electronic structure may be related to the doping-induced band-tailing effects and the observed broad midinfrared optical absorption band. At higher dopings, we show that the conventional phase with fermionic charge carriers has a lower Hartree-Fock energy. This is consistent with the observed transition to a normal metal when the cuprates superconductors are overdoped.

Consider a strongly interacting quasi-two-dimensional electron gas described by the tight-binding Hamiltonian

$$\mathcal{H}=-\sum_{\substack{\langle ij\rangle \\ \sigma}} t_{ij}(a_{i\sigma}^{\dagger}a_{j\sigma}+\text{H.c.})+\sum_{i,j} V_{ij}n_i n_j, \qquad (1)$$

where $a_{i\sigma}^{+}$ creates an electron at site i with spin σ, t_{ij} is the hopping amplitude from site j to site i on the square lattice, $n_i \equiv \Sigma_{\sigma=1}^{2} a_{i\sigma}^{\dagger}a_{i\sigma}$, and V_{ij} is the Coulomb interaction. For nearest-neighbor hopping ($t_{ij}=t_0$) and purely on-site Coulomb repulsion ($V_{ii}\equiv U$), this reduces to the one-band Hubbard model. In order to describe the possibility of spin rotation during the process of electron hopping, we retain the *nearest-neighbor* Coulomb repulsion ($V_{ij}=V$). Using the Pauli spin-matrix identity $\frac{1}{2}\sigma_{\alpha\beta}^{\mu}(\sigma_{\alpha'\beta'}^{\mu})^{*}=\delta_{\alpha\alpha'}\delta_{\beta\beta'}$, it is possible to rewrite the electron-electron interaction terms in the exact form $n_i n_j=(2+\delta_{ij})n_i-\frac{1}{2}\Lambda_{ij}^{\mu}(\Lambda_{ij}^{\mu})^{+}$. Here Λ_{ij}^{μ} are bilinear combinations of electron operators defined by $\Lambda_{ij}^{\mu} \equiv a_{i\alpha}^{\dagger}\sigma_{\alpha\beta}^{\mu}a_{j\beta}$, $\mu=0,1,2,3$. σ^0 is the 2×2 identity matrix, $\vec{\sigma}\equiv(\sigma^1,\sigma^2,\sigma^3)$ are the usual Pauli spin matrices, and there is implicit summation over the repeated indices. The quantum expectation value of the Λ_{ij}^{μ} operators for $i\neq j$ is associated with charge currents ($\mu=0$) and spin currents ($\mu=1,2,3$). Likewise, the quantum expectation value of Λ_{ij}^{μ} for $i=j$ describes the on-site charge density $Q_i=\Lambda_{ii}^{0}$ and the on-site spin-density $S_i^a=\Lambda_{ii}^{a}$, $a=1,2,3$. In the AFM spin-flux model[9–12] we adopt the ansatz that there are no charge density waves (CDW's) or charge currents in the ground state $\Lambda_{ij}^{0}=0$. For positive on-site Hubbard interaction, any CDW would considerably increase the mean-field ground-state energy. Circulating charge currents are accompanied by magnetic fields and have been considered in the context of *conventional* flux phases.[17] However, such states are not observed experimentally in the cuprate superconductors. On the other hand, we incorporate the experimentally observed AFM spin-density background $\langle\vec{S}_i\rangle$ and we postulate the existence of circulating ''spin currents'' that take the form $\langle\Lambda_{ij}^{a}\rangle=(2t_0/V)\Delta_{ij}\hat{n}_a$, where $|\Delta_{ij}|=\Delta$ for all ij and $\hat{n}$ is a unit vector. In the spin-flux phase, these spin currents do not cause any rotation of the local magnetic moments $\langle\vec{S}_i\rangle$. In-

stead, they correspond to rotations in the internal space of Euler angles (phase changes) as the electrons circulate around lattice plaquettes.

Implementing this ansatz with the help of the mean-field factorization $\Lambda^{\mu}_{ij}(\Lambda^{\mu}_{ij})^{+} \rightarrow \langle\Lambda^{\mu}_{ij}\rangle(\Lambda^{\mu}_{ij})^{+} + \Lambda^{\mu}_{ij}\langle\Lambda^{\mu}_{ij}\rangle^{*} + \langle\Lambda^{\mu}_{ij}(\Lambda^{\mu}_{ij})^{+}\rangle - 2\langle\Lambda^{\mu}_{ij}\rangle\langle\Lambda^{\mu}_{ij}\rangle^{*}$ for $i \neq j$ and making the Hartree-Fock factorization for the on-site $i=j$ terms, we obtain the mean-field Hamiltonian

$$\mathcal{H} = \mathcal{H}_{el} + \mathcal{H}_{const},$$

where

$$\mathcal{H}_{el} = -t \sum_{\langle ij\rangle,\alpha\beta} (a^{\dagger}_{i,\alpha} T^{ij}_{\alpha\beta} a_{j,\beta} + \text{H.c.}) - U \sum_{i,\alpha,\beta} a^{\dagger}_{i,\alpha} (\vec{S}_i \cdot \vec{\sigma}_{\alpha,\beta}) a_{i,\beta} + \frac{U}{2} \sum_{i,\alpha} (Q_i - 1) a^{\dagger}_{i,\alpha} a_{i,\alpha} \tag{2}$$

and

$$\mathcal{H}_{const} = U \sum_i \left(\vec{S}_i^2 - \frac{1}{4} Q_i^2 + \frac{1}{2} Q_i \right). \tag{3}$$

Here $T^{ij}_{\alpha\beta} \equiv (\delta_{\alpha\beta} + i\Delta_{ij} \hat{n} \cdot \vec{\sigma}_{\alpha\beta})/\sqrt{1+\Delta^2}$ are spin-dependent SU(2) hopping matrix elements defined by the mean-field theory and $t = t_0\sqrt{1+\Delta^2}$.

In deriving Eq. (2) we have dropped constant terms as well as terms proportional to $\Sigma_i n_i$ obtained from the mean-field factorization of the nearest-neighbor Coulomb interaction. However, we have kept all terms obtained from the Hartree-Fock factorization of the on-site Coulomb repulsion. Thus the entire effect of the nearest-neighbor Coulomb interaction is the renormalization of t and the appearance of the $T^{ij}_{\alpha\beta}$ phase factors in the hopping Hamiltonian.

It was shown previously[9,10] that the ground-state energy of the Hamiltonian of Eq. (2) depends on the SU(2) matrices T^{ij} only through the plaquette matrix product $T^{12}T^{23}T^{34}T^{41} \equiv \exp(i\hat{n} \cdot \vec{\sigma}\Phi)$. Here Φ is the spin flux that passes through each plaquette and 2Φ is the angle through which the internal coordinate system of the electron rotates as it encircles the plaquette. Since the electron spinor wave function is two valued, there are only two possible choices for Φ. If $\Phi = 0$ we can set $T^{ij}_{\alpha\beta} = \delta_{ij}$ and the Hamiltonian (2) describes conventional ordered magnetic states of the Hubbard model. The other possibility is that a spin flux $\Phi = \pi$ penetrates each plaquette, leading to $T^{12}T^{23}T^{34}T^{41} = -1$. This means that the one-electron wave functions are antisymmetric around each of the plaquettes, i.e., that as an electron encircles a plaquette, its wave function in the internal spin space of Euler angles rotates by 2π in response to strong interactions with the other electrons. We call this the spin-flux phase. This uniform spin-flux phase is accompanied by an AFM local moment background (with reduced magnitude) and may be regarded as an alternative mean-field ground state of the conventional AFM phase of the Hubbard model. In the spin-flux phase, the kinetic energy term in Eq. (2) exhibits broken symmetry of a spin-orbit type. This form of spontaneous symmetry breaking occurs over and above that associated with conventional antiferromagnetism. It is also distinct from the smaller, conventional spin-orbit effects that give rise to anisotropic corrections to superexchange interactions between localized spins in the AFM.[18] We emphasize, however, that this AFM mean field is a ''false ground state''[19] at finite doping, analogous to the ''false vacuum'' in early models of quantum chromodynamics.[20] In the presence of charge carriers this mean field is unstable to the proliferation of topological fluctuations (magnetic solitons) that eventually destroy AFM long-range order. In this sense, the analysis that we present below goes beyond simple mean-field theory.

The article is organized as follows. In Sec. II we compare the half-filled AFM mean-field ground states of the conventional phase and the spin-flux phase. We show that the spin-flux phase mean-field ground state always has a lower energy and that it has a single quasiparticle dispersion relation that is consistent with angle-resolved photoemission studies (ARPES). This suggests that the spin-flux phase is a suitable starting point for studying the behavior of the parent compounds upon doping. In Sec. III we consider the problem of adding just one hole to the AFM background. We study in detail two possible soliton excitations, the fermionic, charged, spin bag and the bosonic, charged, meron vortex, for both the conventional and the spin-flux phase. Using a simple energetical argument, we propose a phase diagram for each of these excitations showing which is the relevant excitation for various U/t values and various dopings. In the conventional phase we find that the spin bag is the relevant excitation at all dopings and all values of U/t. In the spin-flux phase, we find that for intermediate U/t values and low dopings, the meron vortices are the relevant excitations. Since the spin-flux phase has the lower energy, this means that a liquid of meron vortices appears on the lattice upon doping. This suggests a plausible explanation for various unusual (non-Fermi-liquid) properties of the underdoped and slightly overdoped cuprate compounds. In Sec. IV we study multisoliton configurations by doping more holes into the lattice. The results obtained are in good agreement with those predicted from the simple phase diagrams inferred in Sec. III. We also show that at higher doping (overdoped samples) the conventional phase has a lower energy than the spin-flux phase and therefore a transition to a conventional Fermi liquid takes place in this regime. Using very simple assumptions, we calculate the optical and static magnetic response of underdoped cuprate containing a frozen liquid of meron vortices and show that it is consistent with the experimental measurements. Finally, Sec. V contains discussion of the results and conclusions.

II. THE UNDOPED MOTT INSULATOR

In order to carry out Hartree-Fock calculations for multisoliton configurations in the antiferromagnet we consider a finite $N \times N$ lattice. In this case the eigenvalues and eigenenergies of the mean-field Hamiltonian can be found numerically and the convergence algorithm is a straightforward iteration procedure. Starting from an initial spin and charge distribution $\vec{S}(i)$ and $Q(i)$ for $i = (i_x, i_y)$ with $i_x = 1,N$ and $i_y = 1,N$, the mean-field Hamiltonian is numerically diagonalized. This in turn leads to new expectation values for the spin and charge distributions given by

$$\vec{S}(i)=\sum_{\alpha=1}^{N_e}\sum_{\sigma,\sigma'=\pm 1}\phi_\alpha^*(i,\sigma)\left(\frac{1}{2}\vec{\sigma}\right)_{\sigma\sigma'}\phi_\alpha(i,\sigma')$$

$$Q(i)=\sum_{\alpha=1}^{N_e}\sum_{\sigma=\pm 1}\phi_\alpha^*(i,\sigma)\phi_\alpha(i,\sigma).$$

Here α is an index for the eigenstates, ϕ_α is the corresponding eigenfunction, and N_e is the total number of electrons on the lattice. This is related to the doping concentration (measured with respect to half filling) by $\delta=1-N_e/N^2$. If the new spin and charge distribution are different from the initial ones, we repeat the diagonalization until self-consistency is reached. In this article, self-consistency is defined by the criterion that the largest variation of any of the charge or spin components on any of the sites is less than 10^{-6} between successive iterations. We assume for simplicity that the mean-field spin-flux parameters T^{ij} are fixed. In a more general theory, these may also be treated as dynamical variables.

It is experimentally observed that the ground state of the undoped Mott insulator has long-range AFM order. Accordingly, we choose a spin distribution of the form $\vec{S}(i)=(-1)^{(i_x+i_y)}S\vec{e}$, where $\vec{e}$ is the unit vector of some arbitrary direction, while the charge distribution is $Q(i)=1$. The results for the conventional AFM are well known. In this case, we choose the Brillouin zone to be a rotated square defined by $-\pi/a\leq k_x+k_y\leq\pi/a$ and $-\pi a\leq k_x-k_y\leq\pi/a$. The dispersion relations are given by

$$E^{\pm}(\vec{k})=\pm E(\vec{k})=\pm\sqrt{\epsilon^2(\vec{k})+(US)^2}, \tag{4}$$

where each level is twofold degenerate and $\epsilon(\vec{k})=-2t[\cos(k_xa)+\cos(k_ya)]$ is the one-electron dispersion relation of the noninteracting conventional state. The mean-field ground-state energy is given by [see Eqs. (2) and (3)]

$$E^{gs}=-2\sum_{\vec{k}}E(\vec{k})+N^2U\left(S^2+\frac{1}{4}\right), \tag{5}$$

where the self-consistent value for the staggered spin S satisfies the energy minimization condition

$$S=\frac{1}{N^2}\sum_{\vec{k}}\frac{US}{E(\vec{k})}. \tag{6}$$

In the spin-flux phase, it is more convenient to choose a square unit cell in order to simplify the description of the T^{ij} phase factors. We make the simplest gauge choice compatible with the spin-flux condition for the T matrices, namely, that $T^{12}=T^{23}=T^{34}=-T^{41}=1$ (see Fig. 1). This leads to a reduced square Brillouin zone $-\pi/2a\leq k_x\leq\pi/2a$ and $-\pi/2a\leq k_y\leq\pi/2a$. The dispersion relations for the AFM configuration are given by

$$E_{sf}^{\pm}(\vec{k})=\pm E_{sf}(\vec{k})=\pm\sqrt{\epsilon_{sf}^2(\vec{k})+(US)^2}, \tag{7}$$

where each level is fourfold degenerate and $\epsilon_{sf}(\vec{k})=-2t\sqrt{[\cos(k_xa)]^2+[\cos(k_ya)]^2}$ are the noninteracting electron dispersion relations in the presence of spin flux. The mean-field ground-state energy is given by

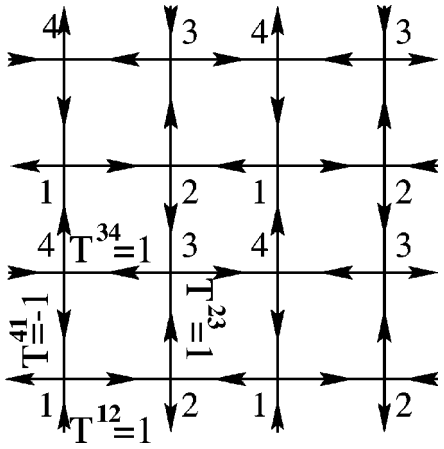

FIG. 1. Choice of the gauge for describing the mean-field spin-flux background. Physical observables depend on the rotation matrices T^{ij} only through the plaquette matrix product $T^{12}T^{23}T^{34}T^{41}$. Shown above is the simplest (spin-independent) gauge choice describing a 2π rotation of the internal coordinate system of the electron (described by three Euler angles) as it encircles an elementary plaquette. This is a different form of spontaneous symmetry breaking for a strongly interacting electron system in which the mean-field Hamiltonian acquires a term with the symmetry of a spin-orbit interaction.

$$E_{sf}^{gs}=-4\sum_{\vec{k}}E_{sf}(\vec{k})+N^2U\left(S^2+\frac{1}{4}\right), \tag{8}$$

where the AFM local moment amplitude is determined by the condition

$$S=\frac{2}{N^2}\sum_{\vec{k}}\frac{US}{E_{sf}(\vec{k})}. \tag{9}$$

In both the conventional and spin-flux phases, a Mott-Hubbard gap of magnitude $2US$ opens between the valence and the conduction bands. However, the Fermi surfaces are very different. In the conventional phase, all the points of the Brillouin surface belong to the nested Fermi surface, while in the spin-flux phase the Fermi surface collapses to four points $(\pm\pi/2a,\pm\pi/2a)$. This means that the introduction of the spin flux leads to a lowering of the energies of all the other points of the conventional nested Fermi surface and thus for a strongly interacting electron system the energy of the entire system is lower in the spin-flux phase. It is interesting to note that the quasiparticle dispersion relation obtained in the presence of the spin flux closely resembles the dispersion as measured through ARPES in a compound such as $Sr_2CuO_2Cl_2$ (Ref. 21) (see Fig. 2). Namely, there is a a peak centered at $(\pi/2,\pi/2)$ with an isotropic dispersion relation around it, observed on both the (0,0) to (π,π) and $(0,\pi)$ to $(\pi,0)$ lines. The spin-flux model at mean field exhibits another smaller peak at $(0,\pi/2)$ that is not resolvable in existing experimental data. This minor discrepancy may be due to next nearest-neighbor hopping or other aspects of the electron-electron interaction that we have not yet included in our model.[22] The quasiparticle dispersion relation of the conventional phase has a large peak at $(\pi/2,\pi/2)$ on the (0,0) to (π,π) line (see Fig. 2), but it is perfectly flat on the $(0,\pi)$ to $(\pi,0)$ line. Also, it has a large crossing from the upper to the lower band

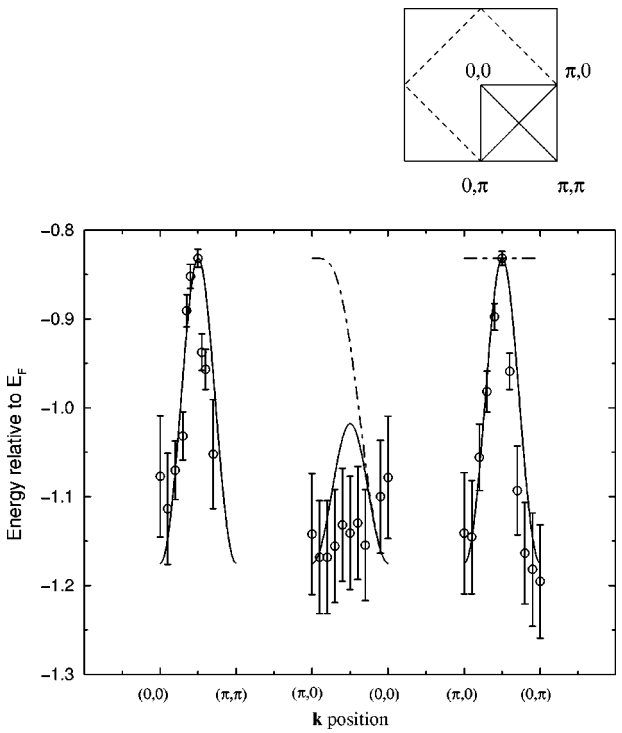

FIG. 2. Comparison between the experimentally determined $E(\vec{k})$ quasiparticle dispersion relation, from angle resolved photoemission studies (ARPES), for the insulating $Sr_2CuO_2Cl_2$ (open circles with error bars) and the mean-field AFM spin-flux phase dispersion relation (full line) and the mean-field AFM conventional phase dispersion relation (dash-dotted line). While the peak on the (0,0) to (π,π) is equally well described in both models, the mean-field spin-flux model gives a much better agreement for the $(\pi,0)$ to (0,0) and $(\pi,0)$ to $(0,\pi)$ directions. The fitting corresponds to $U=2.01$ eV and $t=0.29$ eV for the spin-flux phase and $U=1.98$ eV and $t=0.21$ eV for the conventional phase. The experimental results are the ARPES results of Ref. 21.

edge on the (0,0) to $(0,\pi)$ line. This dispersion relation is very similar to that of the t-J model (see Ref. 22).

The self-consistent solutions of Eqs. (5), (6), (8), and (9) are shown in Figs. 3(a) and 3(b) (continuous lines). Figure 3(a) shows the magnitude of the staggered spin as a function of U/t. In the large U/t limit S goes to 1/2, as expected. In the small U/t limit there is a solution with $S\rightarrow 0$ only for the conventional phase. The spin-flux phase admits an AFM ($S\neq 0$) mean-field solution only for $U/t>3$. The ground-state energies per site are shown in Fig. 3(b) as a function of U/t. The energy of the spin-flux phase is lower than the energy of the conventional phase, suggesting that spin flux provides a better mean-field starting point from which to describe fluctuation effects on the system.

In the large U/t limit, the Hubbard model at half filling is equivalent to the Heisenberg model.[23] This equivalence remains true in the presence of spin flux since the Heisenberg exchange coupling involves only the product of phase factors $T^{ij}T^{ji}=1$,

$$\mathcal{H}=\frac{4t^2}{U}\sum_{\langle i,j\rangle}|T^{ij}|^2\left(\vec{S}_i\vec{S}_j-\frac{1}{4}\right).$$

This equivalence between the conventional and spin-flux phases is indeed observed in all our numerical simulations

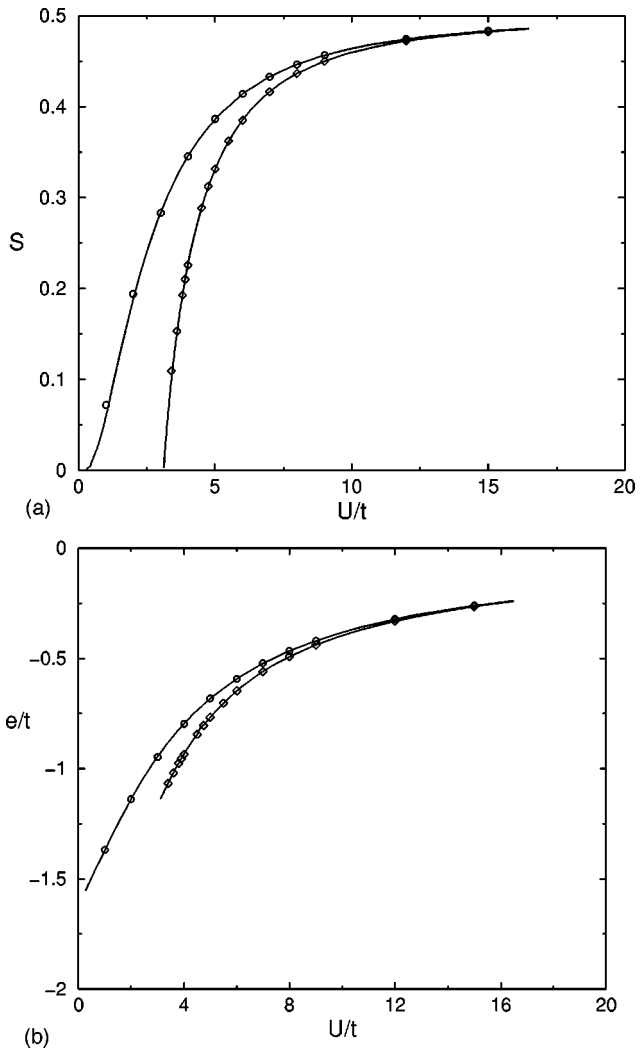

FIG. 3. (a) Dependence of the staggered spin S of the AFM undoped compound with U/t. The diamonds show the numerical results obtained in the presence of the spin flux, while circles show numerical results for the conventional phase. The lines show the values predicted by Eqs. (6) and (9) for the two phases. The spin-flux phase has a mean-field AFM solution ($S\neq 0$) only for $U/t>3$. As expected, $S\rightarrow 1/2$ in the large U/t limit, where every electron becomes localized on individual sites. (b) Dependence of the ground-state energy per site of the AFM parent compound with U/t. The diamonds show the numerical results obtained in the presence of the spin flux, while circles show numerical results for the conventional phase. The lines show the values predicted by Eqs. (5) and (8) for the two phases. The mean-field AFM spin-flux phase has a lower energy than the mean-field AFM conventional phase for all values of U/t.

when the electron concentration is at, or extremely near, half filling. The small differences are due to higher-order virtual hopping corrections to the Heisenberg model. The most significant differences between the spin-flux AFM and the conventional AFM occur at intermediate U/t values.

The analytical results described above provide a useful check for our self-consistent numerical scheme. The circles and diamonds of Figs. 3(a) and 3(b) show the numerical results obtained in the ''bulk'' limit, in good agreement with the analytic results. If we use cyclic boundary conditions (CBC's), which require an even value for N, the bulk limit is reached for $N\geqslant 10$.

III. SOLITONS IN THE DOPED MOTT INSULATOR

When charge carriers are added to the system, the Hamiltonian depends directly on the doping charge through the $Q(i)$ parameters [see Eq. (2)]. As a result we have different mean-field Hamiltonians for hole-doped and electron-doped systems. However, the charge-conjugation symmetry is preserved in the sense that the self-consistent spin and charge distributions, the one-electron spectrum, and total energy of the hole-doped and electron-doped system are very simply related to one another. The correspondence is as follows. Let $\mathcal{H}^h$ be the Hamiltonian of a hole-doped system defined by the parameters $\vec{S}^h(i)$ and $Q^h(i)=1-\rho(i)$, where $\rho(i)$ is the charge distribution of the doping holes. If this Hamiltonian is self-consistent, so is the Hamiltonian $\mathcal{H}^e$ of the electron-doped system defined by the parameters $\vec{S}^e(i)=-\vec{S}^h(i)$ and $Q^e(i)=1+\rho(i)=2-Q^h(i)$. This follows from the fact that if $\phi^h(i)$ is a spinor such that $\mathcal{H}^h\phi^h(i)=E\phi^h(i)$, then $\phi^e(i)=(-1)^{(i_x+i_y)}\phi^h(i)$ satisfies $\mathcal{H}^e\phi^e(i)=-E\phi^e(i)$. In other words, the doping charges are distributed identically (only with different signs) and the final spin configurations are identical, while the electronic spectrum of the hole-doped system is obtained from that of the electron-doped system by reflection with respect to $E=0$. Also, if n is the number of charge carriers (measured with respect to the half-filled system), the energies of the hole-doped and the electron-doped configurations are related by $E_{hole}(n)=E_{electron}(n)-Un$. This difference in the energies of the equivalent hole-doped and electron-doped configurations is entirely an artifact of the absence of a charge term describing the interaction of the electrons with the neutralizing positive background of nuclei. A hole-doped configuration always appears energetically less expensive than the corresponding electron-doped configuration since the latter has additional electron-electron repulsions, with no compensating electron-nuclei attraction. A very simple way of compensating for this is to identify the average energy $[E_{hole}(n)+E_{electron}(n)]/2$ with the energy of the state with n doping charges.

All the spin and charge distributions, as well as electronic spectra presented in the rest of this article, are the ones associated with the corresponding hole-doped systems. For the energies of these configurations we give the average value identified above, unless otherwise stated. However, we emphasize that the difference between the energies of the corresponding hole-doped and electron-doped systems Un is independent of the distribution of the n charges. Therefore, if we compare different configurations corresponding to the same doping and U/t parameter, the hole-doped, electron-doped, and averaged energies lead to the same optimum Hartree-Fock soliton configuration.

A. The spin bag

If we introduce just one hole in the plane, the self-consistent solution we get is a conventional polaron or spin bag (see Figs. 4 and 5). The doping hole is localized around a particular site, leading to the appearance of a small ferromagnetic core around that site. The spin and charge distributions at the other sites are only slightly affected. In fact, the localization length of the charge depends on U/t and becomes very large as $US\rightarrow 0$ since in this limit the Mott-Hubbard gap closes. For intermediate and large U/t, the doping hole is almost completely localized on the five sites of the ferromagnetic core. The static spin configuration surrounding the hole makes charge transport very difficult since motion of the hole outside the ferromagnetic core will create a string of antiferromagnetic bond defects. The hole may circumvent this self-trapped configuration by further twisting the AFM background. However, the subgap electronic level induced by the spin bag ensures that it has a lower Hartree-Fock energy than a hole in the valence band of a spiral (twisted) magnetic background state.

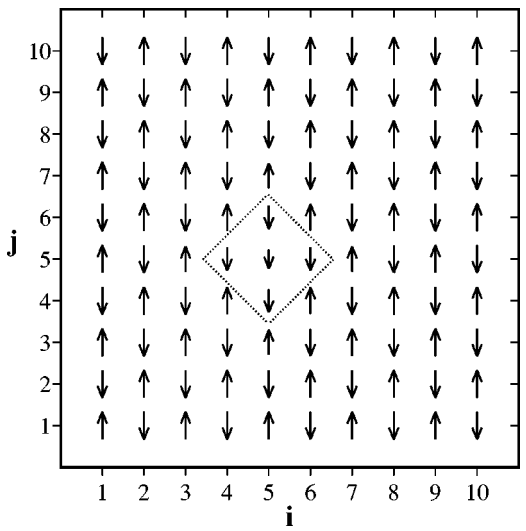

FIG. 4. Self-consistent spin distribution of a 10×10 lattice with a spin bag centered at (5,5). The spin bag has a small ferromagnetic core and the magnetic order is only locally affected.

The spin bag is a charged fermion, as can be seen by direct inspection of its charge and spin distributions (see Figs. 4 and 5). The electronic spectrum in the presence of the hole-doped spin bag [see Figs. 6(a) and 6(b)] reveals that two levels are drawn deep into the Mott-Hubbard gap. These are the first empty levels, suggesting that one of the discrete gap

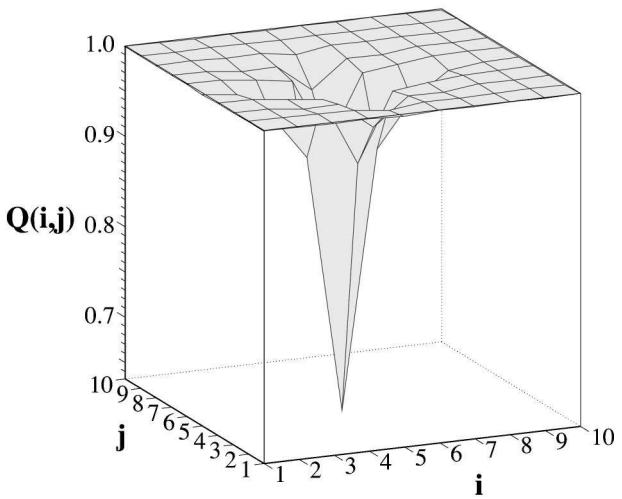

FIG. 5. Self-consistent charge distribution of a 10×10 lattice with a spin bag centered at (5,5). There is an average of one electron per site everywhere, except in the core of the spin bag, where the doping hole is localized.

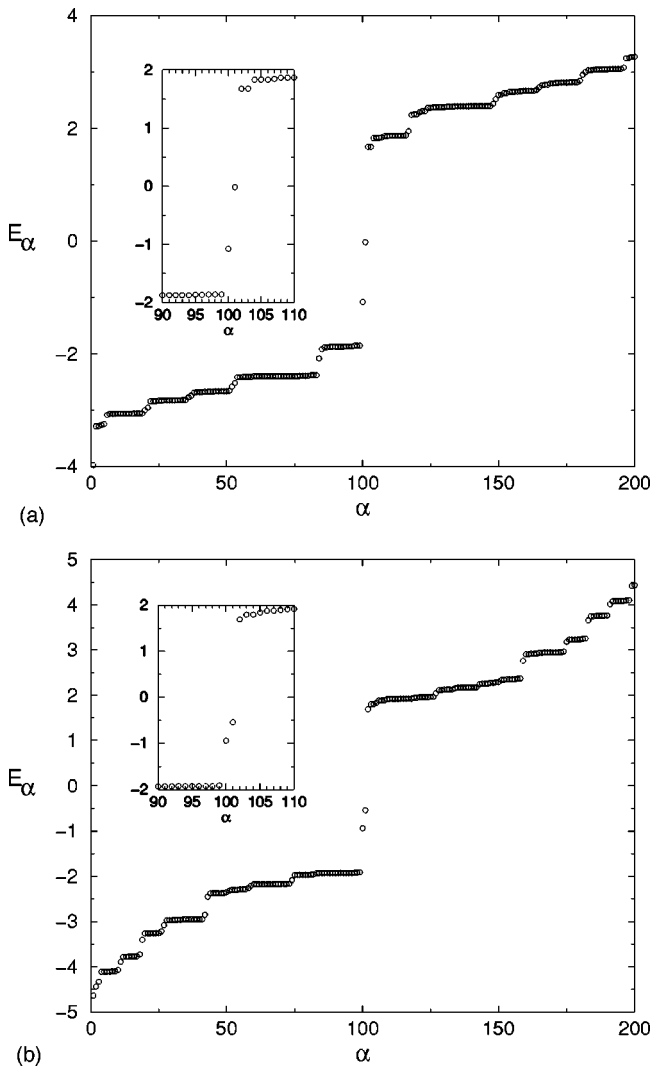

FIG. 6. (a) Electronic spectrum of a spin bag on a 10×10 lattice for $U/t=5$ and spin flux. Eigenenergies E_α are plotted as a function of $\alpha=1,2,\ldots,2N^2$ ($N=10$). Only the first $N^2-1=99$ states are occupied. There are two empty bound discrete levels deep into the Mott-Hubbard gap ($\alpha=100,101$), one of which comes from the valence band of the undoped AFM compound (see inset). There is also an occupied discrete level below the valence band ($\alpha=1$). The valence band is spin paired since it has an even number of levels. Thus the total spin of the spin bag comes from the discrete occupied level. The spin bag is a charged, spin-$\frac{1}{2}$ fermion. (b) Electronic spectrum of a spin bag on a 10×10 lattice for $U/t=5$ in the conventional state. Eigenenergies E_α are plotted as a function of $\alpha=1,2,\ldots,2N^2$ ($N=10$). Only the first $N^2-1=99$ states are occupied. There are two empty bound discrete levels deep into the Mott-Hubbard gap ($\alpha=99,100$), one of which comes from the valence band of the undoped AFM compound (see inset). There are also three occupied discrete levels below the valence band ($\alpha=1,2,3$). The valence band is spin paired since it has an even number of levels. Thus the total spin of the spin bag comes from the discrete occupied levels. The spin bag is a charged, spin-$\frac{1}{2}$ fermion.

levels emerged from the upper edge of the valence band, while the other one emerged from the lower edge of the conduction band. There is also an odd number of occupied discrete levels that split from the lower edge of the valence band (one in the spin-flux case, three in the conventional phase). This means that the valence band continues to have

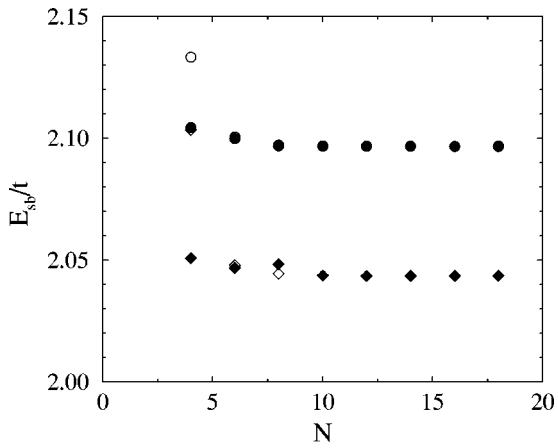

FIG. 7. Excitation energy of a spin bag $E_{spin\ bag}$ as a function of the lattice size N. Diamonds show results for a spin-flux AFM phase, with CBC's (full diamonds) and FBC's (empty diamonds). Circles show results for the conventional AFM state, with CBC's (full circles) and FBC's (empty circles). The Hubbard parameter is $U/t=6$. The bulk limit is reached for $N>10$. In this limit, the excitation energy of the localized spin bag becomes independent of the size of the lattice.

an even (paired) number of levels and therefore its contribution to the total spin is zero. However, the excitation carries the spin localized on the occupied discrete levels. Since there is an odd number of such levels, the spin of the excitation is a half-integer spin.

We define the excitation energy of a spin bag as the difference between the energy of a self-consistent configuration with a spin bag and the energy of the undoped AFM background. In Fig. 7 we show the variation of this excitation energy with the size N of the lattice, for $U/t=6$, for both cyclic and free boundary conditions. As expected, the excitation energy of the spin bag does not depend on the size of the lattice for $N\geqslant10$. The variation of the excitation energy of the spin bag with U/t is shown in Fig. 8. In the very large U/t limit, this energy goes asymptotically from above to

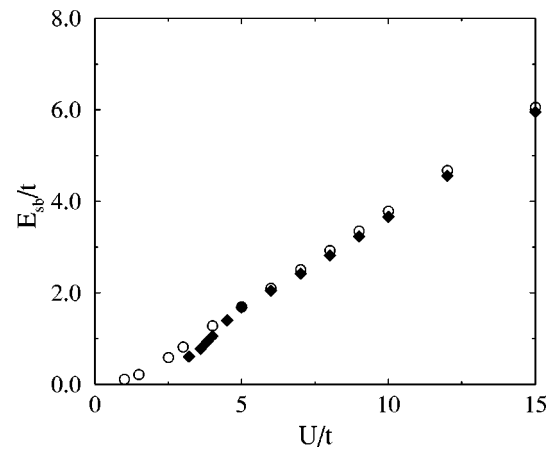

FIG. 8. Excitation energy of a spin bag $E_{spin\ bag}$ as a function of U/t, in the presence of spin flux (filled diamonds) and in the conventional state (circles). In the very large U/t limit, the excitation energy approaches asymptotically the value $U/2-2t$. The excitation energy of a spin bag is lower in the spin-flux phase than in the conventional phase.

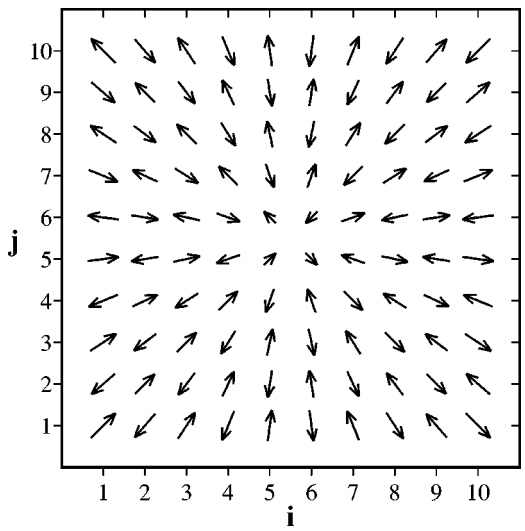

FIG. 9. Self-consistent spin distribution of a 10×10 lattice with a meron vortex in the spin-flux phase. The core of the meron is localized in the center of a plaquette, in the spin-flux phase (in the conventional phase, the core of the meron vortex is localized at a site). This excitation has a topological winding number 1 since the spins on either sublattice rotate by 2π on any curve surrounding the core. The magnitude of the staggered magnetic moments is slightly diminished near the vortex core, but is equal to that of the undoped AFM background far from the core.

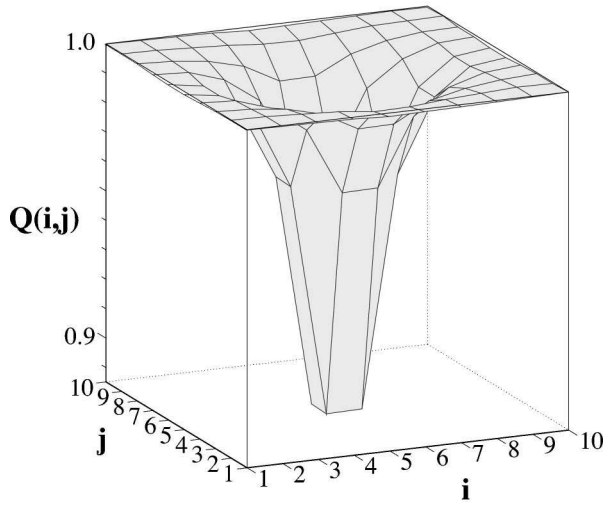

FIG. 10. Self-consistent charge distribution of a 10×10 lattice with a meron vortex in the spin-flux phase. Most of the doping charge is localized in the center of the meron. Far from the core, there is an average of one electron per site.

$U/2-2t$. This can be understood from the fact that in this limit, a hole-doped spin bag should cost no Coulomb energy since we simply remove an electron from a site. An electron-doped spin bag, on the other hand, costs U since we have a doubly occupied site. In both cases, the doping charge can move within the ferromagnetic core, lowering its energy by $2t$. The average energy, therefore, is $U/2-2t$, as obtained numerically.

B. The meron vortex

In the previous discussion it was suggested that the charged spin bag is relatively immobile in the AFM background whereas a twisted magnetic background would facilitate electrical conductivity. In this section we present another self-consistent charged soliton, the meron vortex (see Figs. 9 and 10). This excitation has a topological (winding) number 1 (i.e., the spins on each sublattice rotate by 2π on any closed contour surrounding the center of the meron). As such, this excitation cannot appear alone in an infinitely extended AFM plane by the introduction of a single hole into the plane. From a topological point of view, this is so because the AFM background has a winding number 0 and the winding number must be conserved, unless topological excitations migrate over the boundary into the considered region. Moreover, the excitation energy of the meron vortex diverges logarithmically with the size of the lattice. This means that an isolated hole introduced in the AFM plane is initially dressed into a spin-bag excitation. Nevertheless, we study the characteristics of the isolated meron vortex since this provides a foundation for understanding multiple meron-antimeron configurations at higher dopings, which are no longer topologically or energetically forbidden.

In order to get a self-consistent meron solution, we start with a spin configuration with a winding number of unity. Successive iterations conserve this winding number, but adjust the magnitude of the spins and distribution of charges until self-consistency is reached. In this case, it is useful to use free boundary conditions since cyclic boundary conditions would distort the spins near the edges of the sample such that they orient in the same direction with the spins on the opposite edge, affecting the excitation energy.

From Figs. 9 and 10 we can see that the meron vortex is a charged boson since the total spin of such a configuration is zero, while it carries the doping charge. Its electronic spectrum is shown in Figs. 11(a) and 11(b). In the presence of the hole-doped meron vortex we see a pair of levels drawn deep into the gap. In the conventional AFM state these two levels are degenerate, whereas in the spin-flux phase the degeneracy is lifted. This is a direct consequence of the fact that the self-consistent meron vortex of the spin-flux phase is localized at the center of a plaquette (as shown in Fig. 9) while a self-consistent meron vortex in the conventional state is localized at a site. If the charge-dependent terms are removed from the meron vortex Hamiltonian, this pair of levels is exactly at the midgap of the Mott-Hubbard gap for any value of U/t, as predicted in Ref. 11. These two levels are the first unoccupied levels, suggesting that one of them emerges from the valence band, while the other one emerges from the conduction band. Moreover, they split from the $(\pi/2,\pi/2)$ peaks of the electron dispersion relation (the Fermi points of the spin-flux phase).[11,12] This process is consistent with the opening of the hole pockets near $(\pi/2,\pi/2)$ in the underdoped cuprates.

The bosonic nature of the meron vortex can be inferred from its electronic spectrum as well. In this case [see Figs. 11(a) and 11(b)] only the extended states of the valence band are occupied and therefore they are the only ones contributing to the total spin. Since only one state is drawn from the valence band into the gap, becoming a discrete bound level, it appears that an odd (unpaired) number of states was left in the valence band. However, one must remember that for topological reasons, merons must appear in vortex-antivortex pairs. Thus the valence band has an even number of (paired)

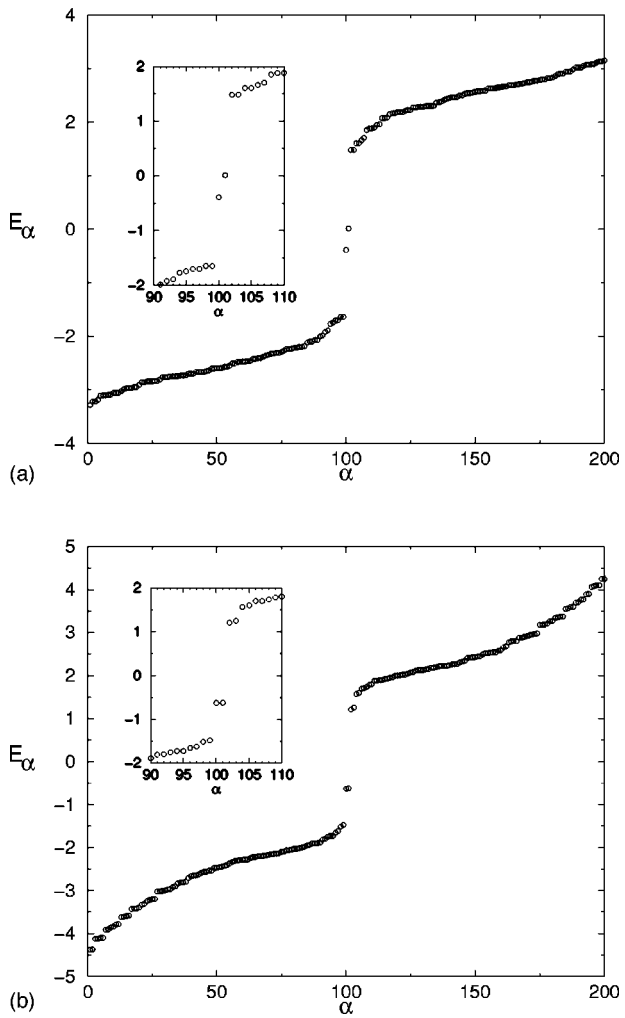

FIG. 11. (a) Electronic spectrum of a meron vortex on a 10×10 lattice, for $U/t=5$, in the presence of the spin flux. Eigenenergies E_α are plotted as a function of $\alpha=1,2,\ldots,2N^2$ ($N=10$). Only the first $N^2-1=99$ states are occupied (the valence band). There are two discrete empty levels deep into the Mott-Hubbard gap, one of which ($\alpha=100$) comes from the valence band of the undoped AFM parent. Merons must be created in vortex-antivortex pairs (for topological reasons). Each pair removes two levels from the undoped AFM valence band. Thus the valence band remains spin paired and the total spin of this excitation is zero. This meron is a spinless, charged, bosonic collective excitation of the doped antiferromagnet. (b) Electronic spectrum of a meron vortex on a 10×10 lattice, for $U/t=5$, in the conventional phase. Eigenenergies E_α are plotted as a function of $\alpha=1,2,\ldots,2N^2$ ($N=10$). Only the first $N^2-1=99$ states are occupied (the valence band). There is a double degenerate unoccupied bound discrete level deep into the Mott-Hubbard gap. One of these bound levels ($\alpha=100$) comes from the valence band of the undoped AFM parent. Merons must be created in vortex-antivortex pairs (for topological reasons). Each pair removes two levels from the undoped AFM valence band. Thus the valence band remains spin paired and the total spin of this excitation is zero.

levels and the total spin is zero. This argument of the bosonic character of the meron vortex is identical to that for the charged domain wall in polyacetylene.[12–14]

The excitation energy of the meron as a function of the lattice size is shown in Fig. 12 for a fixed U/t. This excitation energy was obtained by subtracting the energy of an AFM undoped background (with free boundary conditions) from the energy of the meron-configuration. As in the case of the spin-bag excitation, it is energetically more expensive to excite a meron in the conventional phase than in a spin-flux phase for all possible values of U/t. The dependence of the excitation energy on N may be fitted to the expected form $E_{meron}(N)=\alpha\ln N+\epsilon_{core}$. The dependences of α and ϵ_{core} on U/t are shown in Figs. 13 and 14. Both vanish as $S\to0$ (corresponding to $U\to3t$ for the spin-flux phase and $U\to0$ for the conventional phase). In the very large U limit, $\alpha\to0$ and $\epsilon_{core}\to U/2$, as expected. In this limit all possible spin configurations become degenerate (i.e., there is no difference between the excitation energy of a meron and the excitation energy of a spin bag). In the intermediate U/t

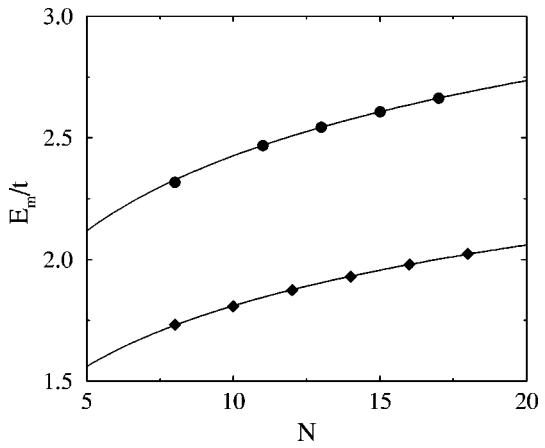

FIG. 12. Excitation energy (in units of t) of a single meron vortex, as a function of the meron size N, in the presence of the spin flux (diamonds) and without spin flux (circles). The lines show fits with a logarithmic dependence on N, $E_{meron}(N)=\alpha\ln N+\epsilon_{core}$. The excitation energy of a meron vortex is always lower in the spin-flux phase than in the conventional phase. If the size of the meron core is small enough, the excitation energy of the meron vortex may become smaller than the excitation energy of a spin bag.

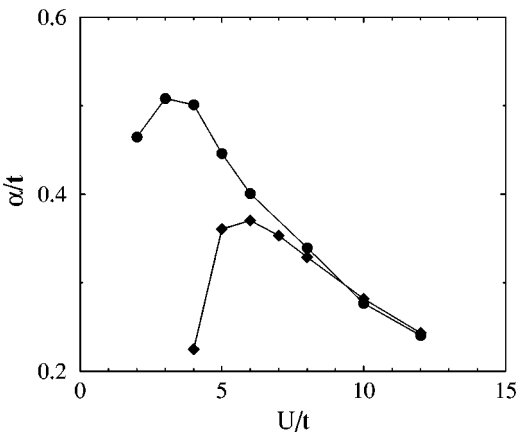

FIG. 13. Dependence of the coefficient α (in units of t) from the fit $E_{meron}(N)=\alpha\ln N+\epsilon_{core}$ on U/t. Diamonds show results for a spin-flux phase, while circles correspond to a conventional state. The line serves to guide the eye. In the large U/t limit $\alpha\to0$ since in this limit all spin configurations become degenerate and the excitation energy of the meron vortex should equal the excitation energy of the spin bag.

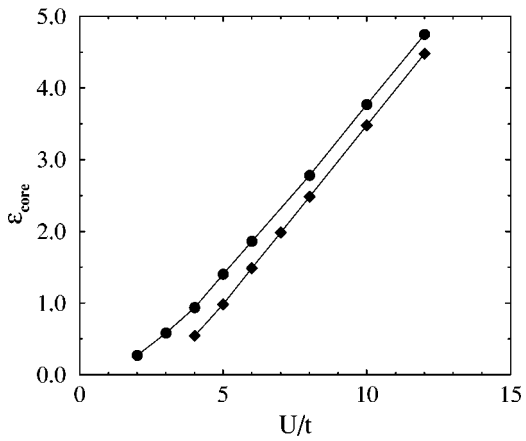

FIG. 14. Dependence of ϵ_{core} (in units of t) from the fit $E_{meron}(N)=\alpha \ln N+\epsilon_{core}$ on U/t. Diamonds show results for a spin-flux phase, while circles correspond to a conventional state. The line serves to guide the eye. In the large U/t limit $\epsilon_{core} \rightarrow E_{spin\ bag}$ since in this limit all spin configurations become degenerate and the excitation energy of the meron vortex should equal the excitation energy of the spin bag.

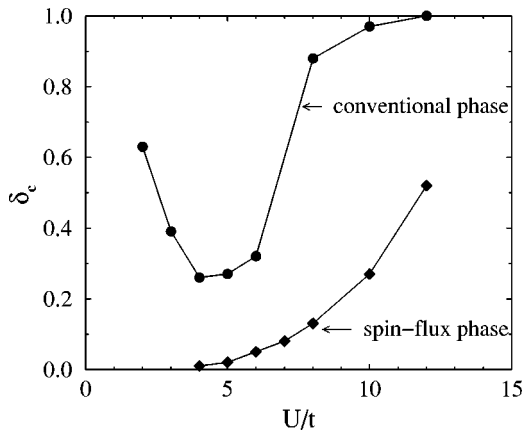

FIG. 15. Critical doping concentration δ_c, above which a charged meron-antimeron liquid is energetically favorable compared to a gas of spin bags. Diamonds show results for a spin-flux phase, while circles correspond to a conventional state. The line serves to guide the eye. In the conventional phase the critical concentrations are very large, $\delta_c>0.3$. In the spin-flux phase the transition to the liquid of meron vortices takes place at dopings smaller than 0.10 for $U/t<8$. In the conventional phase the critical doping is so large ($\delta_c>0.30$) that merons are unlikely to appear before the Mott-Hubbard gap itself closes.

region, the core energy of the meron vortex in the spin-flux phase is energetically less expensive than that of the meron vortex of the conventional phase due to the spreading of its charged core over the four sites of a plaquette.

Comparing the energy of a meron in a finite size sample with that of a spin bag, we can obtain a crude estimate of the critical doping concentration at which a transition from the spin bags to a liquid of charged meron vortices may take place. Comparing Fig. 14 with Fig. 8, we see that $\epsilon_{core} < E_{spin\ bag}$ for small and intermediate U/t. This means that the excitation energy of a meron vortex is smaller than that of a spin bag provided the effective size N_{eff} of the meron is smaller than N_0 defined by $E_{meron}(N_0)=\alpha \ln(N_0)+\epsilon_{core} = E_{spin\ bag}$. The effective size is given by the sample size N or the distance to the core of the nearest antimeron, whichever is smaller. This suggests that for an infinite lattice and finite doping, meron-vortex excitations have lower energies than spin-bag excitations provided each hole is dressed by a meron or antimeron vortex and that the average separation between the vortex and the antivortex is less than N_0. Clearly, this may occur if the doping concentration δ is larger than the critical value $\delta_c \equiv 1/N_0^2$. We plot this critical concentration as a function of U/t in Fig. 15 for both conventional and spin-flux phases.

In the conventional phase we see that the purported critical concentration for the dissociation of spin bags into charged meron-antimeron pairs is larger than 0.30. At such large doping concentrations the average size of the excitation is $N_0<2$ and the distinction between merons and spin bags is blurred. We conclude, therefore, that there is no clear transition from a state with spin-bag excitations to a state with meron excitations as the doping increases. In other words, the only relevant excitations for the conventional AFM phase are spin bags, within the Hartree-Fock approximation.

In the spin-flux phase, the situation is very different. For a broad range of intermediate values of U/t the critical concentration δ_c is small and the distinction between spin bags and merons remains clear. This suggests that for these values of U/t there are two distinct types of Hartree-Fock ground states, as a function of doping. At very low dopings, the spin-bag excitations are energetically more favorable. Since spin bags affect the magnetic order only locally, the long-range AFM order is still preserved in their presence. However, if the concentration increases beyond δ_c, it is energetically favorable for each hole to be surrounded by a meron or antimeron vortex. In this case, the long-range AFM order can be destroyed, leaving behind either power-law decaying magnetic correlations or short-range AFM on the length scale of the average distance between vortices.

In the above estimate of the critical concentration δ_c we assumed that the merons and antimerons are uniformly distributed. However, the actual critical concentration δ_c may be lowered when the tendency of merons and antimerons to form tightly bound pairs (of total winding number 0) is considered. In Figs. 16 and 17 we show the self-consistent spin and charge distributions for the lowest energy configuration found when we put two holes on the AFM lattice in the spin flux phase. It consists of a meron and an antimeron centered on neighboring plaquettes. As a result of the interaction, the cores of the vortices are somewhat distorted and most of the charge is missing from the (10,10) site that is common to both cores. If the vortices were uncharged, a total collapse of the vortex-antivortex pair would be plausible. However, for charged vortices, the fermionic nature of the underlying electrons prevents two holes from being localized at the same site, in spite of the bosonic character of the collective excitation.

A very interesting feature of this tightly bound meron-antimeron solution is that the attraction between the charged vortices is of purely topological nature and appears even though the electronic Hamiltonian (1) contains only repulsive electron interactions. Vortex-antivortex attraction varies as the logarithm of the distance between the cores and therefore the pair of vortices should remain bound even if full Coulomb repulsion exists between the charged cores. Thus

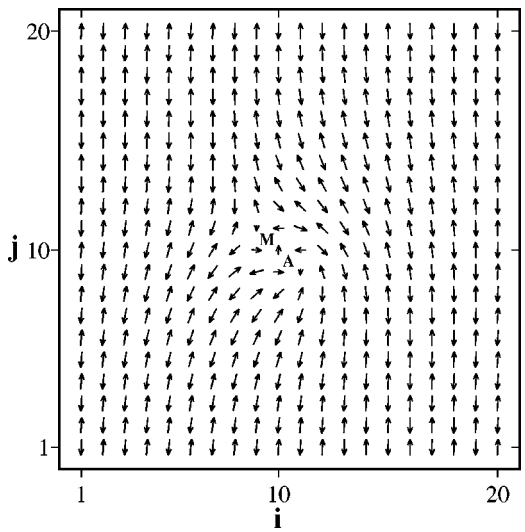

FIG. 16. Self-consistent spin distribution for a tightly bound meron-antimeron pair in the spin flux phase. The meron (M) and the antimeron (A) are localized on neighboring plaquettes. The total winding number of the pair is zero. The magnetic AFM order is disturbed only on the small region where the vortices are localized. The attraction between holes is of topological nature and on a long length scale is stronger than unscreened Coulomb repulsion between charges.

the process of nucleation of meron-antimeron pairs upon doping provides a very natural scenario for the existence of preformed pairs in the underdoped regime.

There is another possible self-consistent state for the system with two holes, consisting of two spin bags far from each other (such that their localized wave functions do not overlap). The excitation energy of such a pair of spin bags is simply twice the excitation energy of a single spin bag. When this excitation energy is compared to the excitation energy of the tightly bound meron-antimeron pair, we find that it is higher by $0.15t$ (for $U/t=5$). This would suggest that spin bags are always unstable to the creation of charged meron-antimeron pairs within the spin-flux phase and that the critical doping concentration δ_c should be set equal to zero. A more realistic determination of the critical hole concentration for the nucleation of meron-antimeron pairs requires the incorporation of the long-range Coulomb repulsion between charge carriers in the doped Mott insulator.

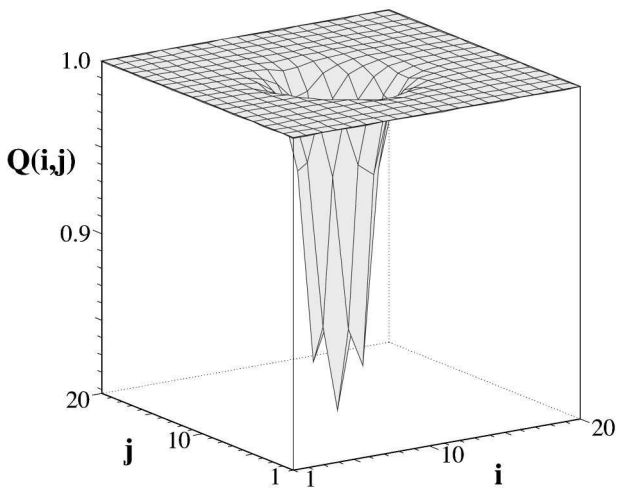

FIG. 17. Self-consistent charge distribution for a tightly bound meron-antimeron pair. The doping charge is mostly localized on the two plaquettes containing the meron and antimeron cores. Due to interactions, the cores of the vortices are somewhat distorted, with most of the charge missing from the (10,10) site common to both cores. The two holes localized in the cores are responsible for the fact that the meron-antimeron pair does not collapse (due to Fermi statistics, it is impossible to have two holes at the same site).

The situation in the high-T_c copper-oxide materials is probably more complex and depends on the nature of the doping process. If the charge carrier concentration is low and uniformly distributed, the average distance between holes is large. At low temperatures, it is possible that these holes are trapped somewhere in the vicinity of their donors in the form of spin bags. If two spin bags encounter each other, they should indeed decay into a tightly bound meron-antimeron pair. Since such a pair distorts the AFM background only in a very small region, magnetic long-range order is preserved. At low temperatures and low dopings, these meron-antimeron pairs may remain pinned to the donor atoms or other forms of disorder, giving rise to the appearance of a spin-glass-type phase of the magnetic background. At higher dopings the pinning potential of the donor atoms is screened and the soliton-soliton interactions are stronger than pinning energies. For concentrations greater than some critical concentration, it is possible that charged meron-antimeron pairs are no longer tightly bound and AFM long-range order is completely destroyed.

If this scenario is applicable to the high-T_c copper oxide materials, it is tempting to associate the charge carriers in the doping regime relevant to superconductivity with meron vortices. Besides the magnetic order, another extremely important issue is the dynamics of solitons. For instance, in the intermediate U/t regime, a spin bag as depicted in this model (see Figs. 4 and 5) is basically immobile since moving would mean leaving behind a string of ferromagnetically aligned spins. It is plausible[24] that the kinetic energy of localization of the hole could be lowered if the spin bag (spin polaron) has a ferromagnetically aligned core, within which the hole is free to move. Another possibility[25] is that a spiral twist in the AFM background accompanies the hole as it moves. The meron vortex may be regarded as a self-consistent realization of the twist-accompanied hole that is topologically stable even when the charge carrier is stationary. The vortex in the AFM background surrounding the hole facilitates mobility of charge since hopping of the vortex core to a neighboring plaquette leads to a less severe distortion of the AFM exchange coupling between neighboring spins. Since meron vortices have a bosonic nature, the non-Fermi-liquid nature of the metal from which superconductivity emerges is also quite natural.

IV. HIGHER DOPINGS: MULTISOLITON CONFIGURATIONS

For higher carrier concentrations, there is some arbitrariness in choosing the initial spin and charge configurations from which to begin the iterative self-consistency scheme. Since a variety of different self-consistent states may be realized starting from different initial configurations, we adopt a probabilistic approach. We give random numbers as the

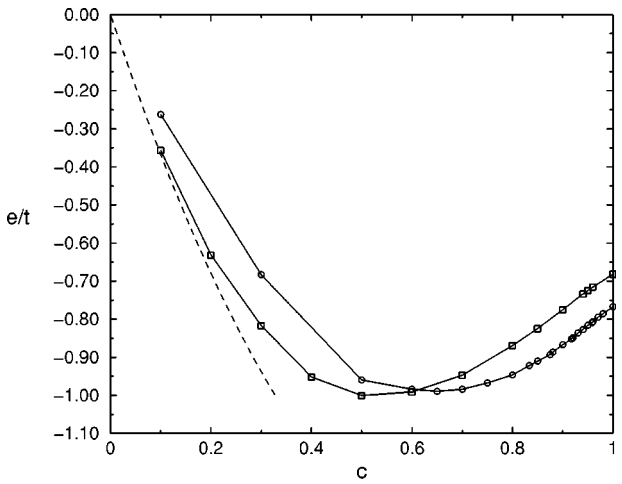

FIG. 18. Energy per site (in units of t) as a function of the electron concentration $c=1-\delta$ for $U/t=5$. Circles correspond to the lowest energies found in the random trial in the spin-flux phase (liquid of meron vortices), while squares correspond to the best result of the random trial in the conventional phase (stripes). The dashed line shows the exact value for $U=0$ (noninteracting case). At low doping (high electron concentration) the liquid of meron vortices of the spin-flux phase has a lower energy than the stripes of the conventional phases. However, at higher dopings ($\delta>0.4$) the conventional phase becomes stable.

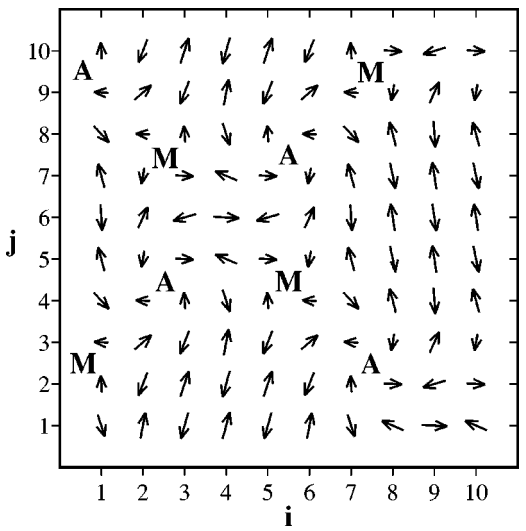

FIG. 19. Self-consistent spin distribution for the configuration of lowest energy found at $\delta=0.08$ (eight holes), starting from an initial random distribution, for $U/t=5$ in the spin-flux phase. Four meron-antimeron pairs appear. We have marked with M the plaquettes on which merons are centered and with A the plaquettes on which antimerons are centered. A meron and an antimeron are ''split'' between the two opposing boundaries (we have imposed cyclic boundary conditions).

initial components of the spin distribution and also choose randomly the sites where the holes are initially localized. This iterative process is repeated many times and the self-consistent configuration of lowest energy is finally selected. As we mentioned before, the relation between the energy per site of the hole-doped configuration and that of the equivalent electron-doped configuration is given by $e_{hole}(\delta)=e_{electron}(\delta)-U\delta$, where δ is the average number of charge carriers per site. For convenience, we plot the energy of the hole-doped configurations as a function of doping. The results obtained in the random searches are summarized in Fig. 18, where the energy per site (in units of t) of the self-consistent hole-doped configurations is plotted as a function of the electron concentration. They correspond to $U/t=5$ and a 10×10 lattice with cyclic boundary conditions. For $\delta=0.01$ and 0.02 (corresponding to one and two holes, respectively) we recapture the results presented in Sec. III. In the spin-flux phase, a single isolated hole forms a spin bag, whereas the lowest energy configuration found for two holes is the tightly bound meron-antimeron pair shown in Figs. 16 and 17. For two holes we also find a number of self-consistent metastable states, containing widely separated spin bags.

For a doping up to about 0.30 (which corresponds to an electron density $c=0.70$–1), the lowest energy configurations always correspond to various arrangements of meron-antimeron pairs in the spin-flux phase. As an example, we show the spin configuration of lowest energy found for eight holes, $c=0.08$ (see Fig. 19). We can see four meron-antimeron pairs arranged such that each meron is surrounded by antimerons and vice versa. This state appears to be a crystal of meron-antimeron pairs, in the sense that the lattice obtained through translations of the 10×10 lattice shown in Fig. 19 has an ordered distribution of meron-antimeron pairs. This crystallization is very likely an artifact of the zero-temperature, semiclassical, static Hartree-Fock approach. Incorporation of dynamics and fluctuations in the model may lead to the melting of this crystal into a quantum liquid of mobile meron-antimeron pairs. However, as discussed in Sec. IV A, ordered arrays of merons and antimerons may play an important role at some special dopings.

As the doping becomes larger than 0.20, the density of vortices is so large that we obtain configurations that have a meron or antimeron vortex localized on almost each plaquette, leading to a state where long-range AFM correlations are completely lost. As a consequence, the doping charge is quite uniformly distributed over the whole lattice and the magnitude of the staggered spin decreases considerably. The apparent overlap of the charge carrier wave functions here suggests that quantum corrections to the Hartree-Fock approximation may be substantial in this doping range and that the charge carriers here form a different type of quantum liquid. Finally, at very large doping ($\delta>0.4$), the entire spin-flux phase is energetically unstable to the formation of a conventional electron gas. This is expected since [see Eqs. (4) and (7)] the bottom of the valence band in the spin-flux phase is higher than that of the valence band in the conventional phase. At very low electron concentrations, the energy per site approaches that of the noninteracting ($U=0$) electron model (see Fig. 18), as expected.

In contrast to the above picture of a meron liquid in the spin-flux phase, the lowest energy configurations at low dopings in the conventional AFM phase always consists of charged stripes.[26,27] For example, in Fig. 20 we show the self-consistent spin configuration found for $c=0.15$, where all the spin bags assemble in a closed stripe (the stripe must close due to the cyclic boundary conditions). We have also calculated the energies of ordered horizontal and diagonal stripes. This necessitates bigger lattices, so that the cyclic

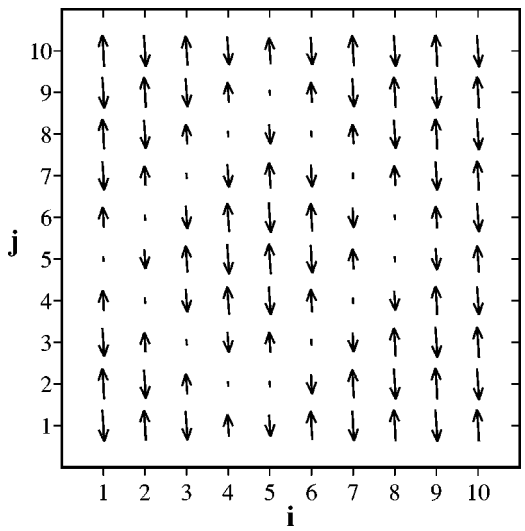

FIG. 20. Self-consistent spin distribution for the configuration of lowest energy found at $\delta=0.15$, starting from initial random distributions, for $U/t=5$ in the conventional phase. A closed charged stripe appears (cyclic boundary conditions were imposed). The AFM order is switched from one phase to the other one (up to down and vice versa) as the stripe is crossed.

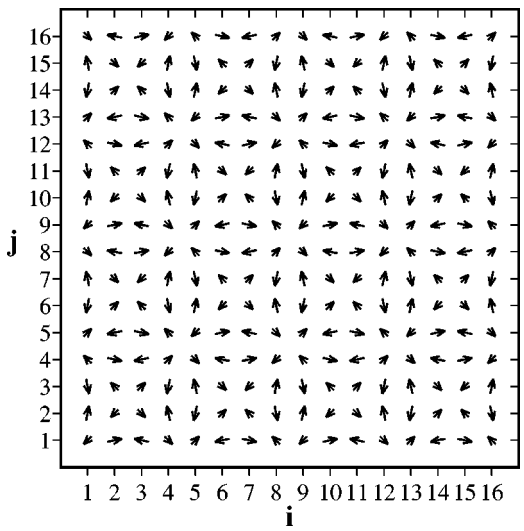

FIG. 21. Self-consistent spin distribution for the configuration of lowest energy found at $\delta=1/8$ for $U/t=5$ in the spin-flux phase. An ordered crystal of charged merons and antimerons is created.

boundary conditions are satisfied. For $U/t=5$ we find basically no difference between the energies of such stripes and that of the closed stripes obtained from the random initial conditions. The instability of the spin bags to stripe formation has also been proved in the three-band Hubbard model and the t-J model.[28] However, as seen from Fig. 18, such states have higher energies than the liquid of meron-antimeron pairs of the spin-flux phase. We have also tried to obtain horizontal and diagonal stripes in the spin-flux phase by starting with an initial configuration containing such a stripe. However, they converge to the liquid of meron-antimeron pairs rather than self-consistent stripe configurations.

At large dopings, the conventional phase becomes energetically more favorable and more and more discrete levels are drawn into the Mott-Hubbard gap. Due to overlap of the charge carrier wave functions, these levels spread into a broad impuritylike band. Also, the staggered magnetization S at each site is strongly suppressed, leading to shifts of the band-edge energies (roughly given by $\pm US$). These two effects conspire to close the Mott-Hubbard gap and lead to the formation of a conventional Fermi liquid with a partially filled band for dopings $\delta>0.3$.

In summary, our picture is that of three distinct regimes. At very low dopings, we have a collection of tightly bound meron-antimeron pairs and/or spin bags, which preserve the long-range AFM order. When the doping exceeds some critical value δ_c, a transition to a quantum liquid of meron-antimeron pairs occurs and is accompanied by the destruction of the AFM long-range order. Since these charged merons are spinless bosons this metallic state will invariably exhibit non-Fermi-liquid properties. As the doping further increases, the spin-flux state itself is unstable, the Mott-Hubbard gap closes, and the system reverts to a conventional Fermi liquid. Although our static Hartree-Fock analysis points to the above picture, it does not describe soliton dynamics and quantum fluctuation effects pertinent to the quantum liquid phase of merons. In addition, a more careful treatment of the long-range part of the Coulomb repulsion between charge carriers may be needed in the non-Fermi-liquid phase where the conventional arguments of screening are inapplicable.[29] Finally, a more realistic model must include the interactions of the doping charges with the impurity charges located in nearby planes and the influence of structural distortions of the CuO planes. The last issue is pertinent to the meron crystal phase at the special doping $\delta=1/8$, which we discuss below.

A. Charge carrier concentration of $\delta=1/8$

The $\delta=1/8$ doping is very special because in some compounds[30] superconductivity is completely suppressed at this doping. A very simple and natural explanation of this suppression is that the charge carriers become immobile. Within our picture of a charged meron liquid, at a doping of 1/8, we find a self-consistent structure consisting of a crystal of merons and antimerons (see Figs. 21 and 22). Neutron scattering reveals that for $\delta=1/8$, the $(\pi/a)(1,1)$ AFM magnetic peak splits into four peaks situated at $(\pi/a)(1,1\pm\frac{1}{8})$ and $\pi/a(1\pm\frac{1}{8},1)$.[31,32] For the calculated meron crystal shown in Figs. 21 and 22, the magnetic structure factor exhibits four peaks with the correct distances between the peaks. However, they are rotated by 45° (they appear along the diagonals, not along the horizontals) relative to the observed neutron scattering peaks. This picture can be brought into agreement with experiments by introducing a small anisotropy in the electron hopping within the copper-oxide plane. The addition of such a perturbation to our model is justified by the experimentally observed distortion of the lattice from the usual low-temperature orthorhombic structure to the low-temperature tetragonal (LTT) structure at this doping.[33] In the LTT structure the atomic displacements form a horizontal (or vertical) structure and very likely favor the pinning of horizontal (vertical) stripes. The easiest way to mimic this structural distortion is to add a small anisotropy in the magnitude of the hopping integral, with the same periodicity. For a 3% anisotropy, the half-filled stripe struc-

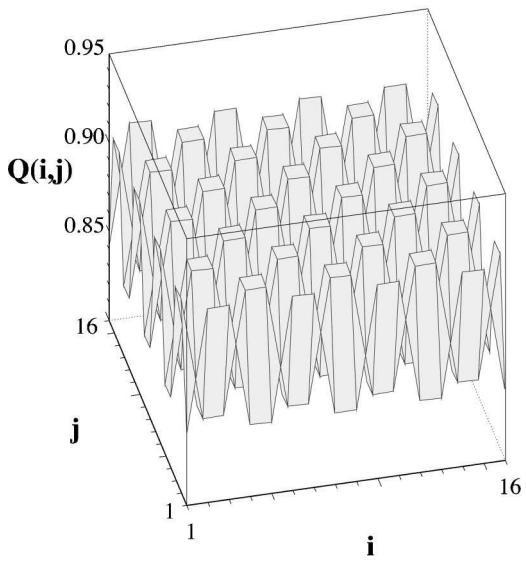

FIG. 22. Self-consistent charge distribution for the configuration of lowest energy found at $\delta = 1/8$ for $U/t = 5$ in the spin-flux phase. An ordered crystal of charged merons and antimerons is created.

ture predicted by Tranquada *et al.*[32] becomes stable (see Fig. 23). The self-consistent stripe configuration obtained in the presence of the small anisotropy is made up of merons and antimerons packed along horizontal lines. This example illustrates that a more realistic model including the effects of such structural distortions and possibly the interaction with the impurity charges is required for a quantitative comparison with experiments.

B. Optical absorption

As we mentioned before, in the presence of each meron or antimeron vortex, two electronic levels, one from the valence band and one from the conduction band, are drawn deep into the gap. In the presence of multisoliton interactions these

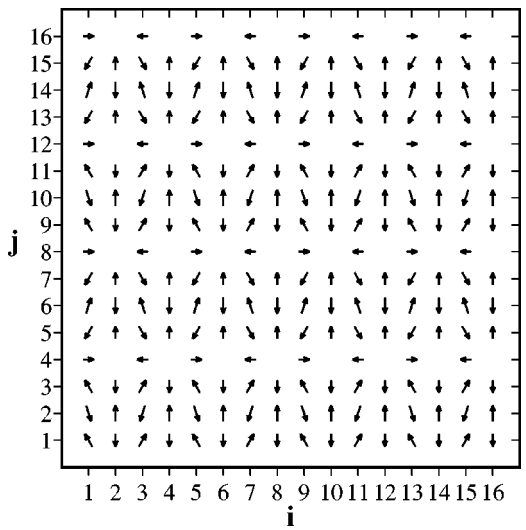

FIG. 23. Self-consistent spin distribution for the configuration of lowest energy found after adding a 3% anisotropy in the hopping integral, at $\delta = 1/8$, for $U/t = 5$ in the spin-flux phase. The merons and antimerons rearrange on horizontal lines, leading to a structure similar to that suggested by Tranquada *et al.* in Ref. 32.

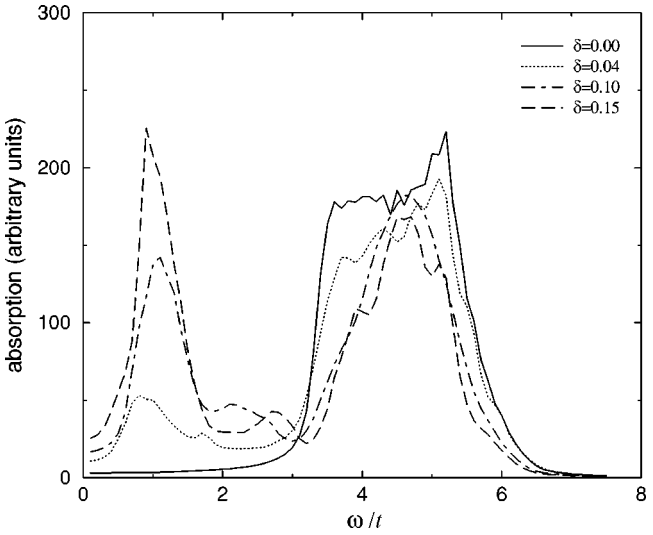

FIG. 24. Optical absorption (arbitrary units) as a function of the frequency (in units of t) for various dopings. The Hubbard parameter is $U/t = 5$ and the corresponding self-consistent lowest-energy configurations of frozen liquids of merons and antimerons were used. The damping coefficient is $\Gamma = 0.1t$. As the doping increases, a broadband due to electronic excitations from the lower Mott-Hubbard gap to the discrete, empty, meron-induced levels develops deep in the gap.

levels spread into a broad impurity band within the larger Mott-Hubbard gap. Since these localized states are empty (for the hole-doped system), electrons can be optically excited to them from the valence band. Consequently, a broad optical absorption band appears inside the Mott-Hubbard gap. In Fig. 24 we show the evolution of the optical absorption with doping. The absorption was calculated through straightforward perturbation theory, after a term coupling the doping charge to an external vector field[34] was added to the mean-field Hamiltonian. This leads to the formula for the electric conductivity tensor

$$\sigma_{ij}(\omega) = \frac{1}{i\omega} \sum_{\alpha=1}^{N_e} \sum_{\beta=N_e+1}^{N^2} \left[\frac{\eta^i_{\alpha\beta}\eta^j_{\beta\alpha}}{\hbar\omega - (E_\alpha - E_\beta) + i\Gamma} - \frac{\eta^i_{\beta\alpha}\eta^j_{\alpha\beta}}{\hbar\omega + (E_\alpha - E_\beta) + i\Gamma} \right],$$

where

$$\vec{\eta}_{\alpha\beta} = \frac{iet}{\hbar} \sum_{\langle i,j \rangle} [(\vec{r}_j - \vec{r}_i)\phi^*_\alpha(i)T^{ij}\phi_\beta(j) + (\vec{r}_i - \vec{r}_j)\phi^*_\alpha(j)T^{ji}\phi_\beta(i)]$$

is the matrix element between an occupied state α and an empty state β of the density of current operator $\vec{j}$. Here N_e is the number of occupied states, N^2 is the total number of states, and Γ is a phenomenological damping coefficient. The calculation is approximate, in the sense that we did not include the variation of the spin and charge distributions due to the modification of the wave function in the external field. A more detailed calculation involving a time-dependent generalization of the Hartree-Fock method (the random-phase approximation) will be presented elsewhere. In order to

mimic the interaction with spin waves and other damping effects on the excited electronic states we assumed that the subgap levels are homogeneously broadened with a spectral width of $\Gamma = 0.1t$. This leads to a smooth optical absorption even for a 10×10 lattice. As the doping increases, two effects are apparent. The first is the appearance of a broad absorption band deep into the gap. This is due to the soliton gap states and significant weight is transferred into it from the conduction band. The second effect is that the overall charge-transfer gap itself decreases since doping decreases the average self-consistent value of S, leading to a shift in the mean-field position of the valence- and conduction-band edges. This second effect is less apparent in Fig. 24, because of the fairly large damping we chose. It is well known that the optical absorption of the doped compounds contains a broad midinfrared band and a Drude-like tail starting from very low frequencies.[6] It is reasonable to associate the broad midinfrared band with electronic transitions from the valence band to the vortex mediated impurity band (see Fig. 24). On the other hand, the Drude tail component is associated with the translational motion of the bosonic meron-vortices. This may be described in a time-dependent Hartree-Fock approximation.

C. The magnetic structure factor

We can characterize the evolution of the magnetic long-range order with the doping by looking at the magnetic structure factor. We have calculated the static magnetic structure factor

$$S(\vec{Q}) = \frac{1}{N^2} \sum_{i,j} e^{i\vec{Q}\cdot(\vec{r}_i - \vec{r}_j)} \vec{S}(i)\vec{S}(j),$$

assuming that the spins are frozen in the self-consistent configuration. The results are shown in Fig. 25. The AFM parent compound has a large peak at $(\pi/2, \pi/2)$, as expected. As the doping increases, this peak splits into four incommensurate peaks, whose positions shift with the doping. This is in agreement with the observed behavior of some cuprate compounds.[31,32]

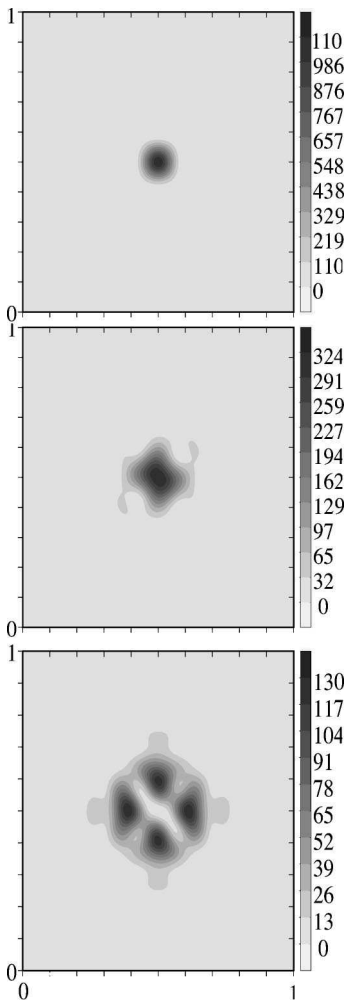

FIG. 25. Static magnetic structure factor as a function of (k_x, k_y), measured in units of $2\pi/a$. The first picture corresponds to $\delta = 0.00$ and has the large magnetic peak at $(\pi/a, \pi/a)$. As the doping increases to $\delta = 0.05$ (second picture) and $\delta = 0.08$ (third picture) this magnetic peak splits into four incommensurate satellites. The Hubbard parameter is $U/t = 5$ and the corresponding self-consistent lowest-energy configurations of frozen liquids of merons and antimerons were used.

V. DISCUSSION AND CONCLUSIONS

In this article we presented a numerical study of a mean-field approximation of the one-band extended Hubbard model. We have shown that at low dopings, the spin-flux phase provides a better starting point than the conventional phase. For U/t in the intermediate range, the lowest energy configurations found in the doping regime relevant to superconductivity consist of a liquid of meron and antimeron vortices. These meron vortices are mobile, charge carrying bosons that accommodate each of the doping holes in an impurity band that occurs within the Mott-Hubbard charge transfer gap. The key ingredient that distinguishes our model from previous studies of the Hubbard model is the concept of spin flux. In its absence, our analysis reproduces the conventional AFM, in which there is a tendency for stripe formation at low doping, as predicted by many other authors.[26–28] However, introduction of spin flux into the AFM leads to a lower mean-field energy state, in which the doping holes find it energetically favorable to be cloaked by vortices of the magnetic background. This cloaking stabilizes the magnetic vortex and also facilitates the mobility of holes in the AFM background. At extremely low doping the holes either are paired in tightly bound meron-antimeron pairs or become spin bags (which may be thought of as a collapsed charged-meron–neutral-antimeron pair). Increasing doping creates a liquid of meron-antimeron pairs, completely destroying AFM order. This picture is consistent with angle-resolved photoemission studies of the quasiparticle dispersion relation, the appearance of a broad midinfrared optical absorption band with doping, and various aspects of the neutron scattering data. It also offers a microscopic mechanism for the non-Fermi-liquid characteristic of the metallic state from which superconductivity emerges.

One of the great challenges in the understanding of charge

carrier pairing is that an attractive force must emerge from a purely repulsive many-electron Hamiltonian. This problem is exacerbated by the fact that the standard arguments of screening of the Coulomb repulsion are based on Fermi-liquid theory and may be inapplicable to a doped Mott insulator. Our model, based on charged vortex solitons, provides a very natural strong attractive force between charge carriers that is of topological origin and can lead to binding of charge carriers even in the absence of screening. Moreover, the presence of vortices in the AFM background will lead to a large renormalization of the spin-wave spectrum. This may in turn be related to the observed pseudogap phenomenon in the high-T_c cuprates.[35] As the doping increases further, the spin-flux phase is unstable to the formation of a conventional Fermi liquid, in which the Mott-Hubbard gap is closed.

All of our results so far are based on a static Hartree-Fock mean-field theory. In spite of the simplicity of our approximation, the calculated properties of our model are consistent with a variety of independent experimental signatures of the cuprate superconductors. We believe that it is reasonable to proceed beyond this mean-field theory to understand in greater detail the quantum and dynamical properties of the meron liquid. The long-range part of the Coulomb repulsion between doping charges may play a more important role in the properties of this quantum liquid than it does in a conventional Fermi liquid where standard screening arguments apply. Also, additional interactions such as crystal field effects and the conventional spin-orbit interaction,[18] which help to stabilize uncharged meron vortices, may need to be added in the starting Hamiltonian (1). These considerations may in turn shed light on the microscopic mechanism of high-temperature superconductivity and the detailed characteristics of the non-Fermi-liquid state from which it arises.

ACKNOWLEDGMENTS

We are grateful to Dr. Vladimir Stephanovich for a number of stimulating discussions and to Dr. Dirk Morr for drawing our attention to the recent ARPES data for $Sr_2CuO_2Cl_2$. This work was supported in part by the Natural Sciences and Engineering Research Council of Canada. M.B. acknowledges support from the Ontario Graduate Scholarship Program.

[1] P.W. Anderson, Science **235**, 1196 (1987).
[2] P.W. Anderson and J.R. Schrieffer, Phys. Today **44** (6), 55 (1991).
[3] J.G. Bednorz and K.A. Muller, Z. Phys. B **64**, 189 (1986).
[4] Y. Iye, in *Physical Properties of High Temperature Superconductors III* (World Scientific Press, Singapore, 1992).
[5] H. Alloul, in *Proceedings of the 39th Scottish Universities Summer School in Physics*, St. Andrews, edited by D. P. Tunstall and W. Barford (Adam Hilger, New York, 1991).
[6] D.B. Tanner and T. Timusk, in *Physical Properties of High Temperature Superconductors III*, edited by Donald M. Ginsburg (World Scientific Press, Singapore, 1992); G.A. Thomas, in *High Temperature Superconductivity*, Proceedings of the 39th Scottish Universities Summer School in Physics, St. Andrews (Ref. 5), p. 169.
[7] See, for instance, D.M. Ginzburg, *Physical Properties of High Temperature Superconductors* (World Scientific Press, Singapore, 1992), Vol. I-V.
[8] See, for instance, D.P. Tunstall and W. Barford, in *High Temperature Superconductivity*, Proceedings of the 39th Scottish Universities Summer School in Physics, St. Andrews (Ref. 5).
[9] S. John and A. Golubentsev, Phys. Rev. Lett. **71**, 3343 (1993); Phys. Rev. B **51**, 381 (1995).
[10] S. John and A. Müller-Groeling, Phys. Rev. B **51**, 12 989 (1995).
[11] S. John, A. Golubentsev, and M. Berciu, Europhys. Lett. **41**, 31 (1998).
[12] M. Berciu and S. John, Phys. Rev. B **57**, 9521 (1998).
[13] A.J. Heeger, S. Kivelson, J.R. Schrieffer, and W.-P. Su, Rev. Mod. Phys. **60**, 781 (1988).
[14] W.-P. Su, J.R. Schrieffer, and A.J. Heeger, Phys. Rev. B **22**, 2099 (1980).
[15] D.J. Gross, Nucl. Phys. B **132**, 439 (1978).
[16] J. Kosterlitz and D. Thouless, J. Phys. C **6**, 1181 (1973); **7**, 1046 (1974).
[17] I. Affleck and B. Marston, Phys. Rev. B **37**, 3774 (1988); B. Marston and I. Affleck, *ibid.* **39**, 11 538 (1989); G.B. Kotliar, *ibid.* **37**, 3664 (1988).
[18] N.E. Bonesteel, T.M. Rice, and F.C. Zhang, Phys. Rev. Lett. **68**, 2684 (1992).
[19] S. Coleman, *Aspects of Symmetry* (Cambridge University Press, Cambridge, 1985).
[20] C. Callan, R. Dashen, and D. Gross, Phys. Lett. **66B**, 375 (1977).
[21] B.O. Wells, Z.-X. Shen, A. Matsuura, D.M. King, M.A. Kastner, M. Greven, and R.J. Birgeneau, Phys. Rev. Lett. **74**, 964 (1995).
[22] P.W. Leung, B.O. Wells, and R.J. Gooding, Phys. Rev. B **56**, 6320 (1997).
[23] P.W. Anderson, Phys. Rev. **115**, 2 (1959).
[24] Y. Nagaoka, Phys. Rev. **147**, 392 (1966).
[25] B.I. Shraiman and E.D. Siggia, Phys. Rev. B **40**, 9162 (1990).
[26] D. Poilblanc and T.M. Rice, Phys. Rev. B **39**, 9749 (1989); H.J. Schultz, J. Phys. (Paris) **50**, 2833 (1989).
[27] M. Kato, K. Machida, H. Nakanishi, and M. Fujita, J. Phys. Soc. Jpn. **59**, 1047 (1990); K. Machida, Physica C **158**, 192 (1989).
[28] J. Zaanen and O. Gunnarson, Phys. Rev. B **40**, 7391 (1989); J. Zaanen, M.L. Horbach, and W. van Saarloos, *ibid.* **53**, 8671 (1996).
[29] V.J. Emery and S.A. Kivelson, Physica C **209**, 597 (1993); **235-240**, 189 (1994); in *Proceedings of the Los Alamos Symposium on Strongly Correlated Electronic Materials, 1993*, edited by K.S. Bedell (Addison-Wesley, Reading, MA, 1994).
[30] A.R. Moodenbaugh, Y. Xu, M. Suenaga, T.J. Folkerts, and R.N. Shelzen, Phys. Rev. B **38**, 4596 (1988).
[31] S.-W. Cheong, G. Aeppli, T.E. Mason, H. Mook, S.M. Hayden, P.C. Canfield, Z. Fisk, K.N. Clausen, and J.L. Martinez, Phys. Rev. Lett. **67**, 1791 (1991); G. Shirane, R.J. Birgeneau, Y. Endoh, and M.A. Karstner, Physica B **197**, 158 (1994); T.E. Mason, G. Aeppli, and H.A. Mook, Phys. Rev. Lett. **68**, 1414 (1992).
[32] J.M. Tranquada, B.J. Sternlieb, J.D. Axe, Y. Nakamura, and S. Uchida, Nature (London) **375**, 561 (1995).

[33] M.K. Crawford, R.L. Harlow, E.M. McCarron, W.E. Farneth, J.D. Axe, H. Chou, and Q. Huang, Phys. Rev. B **44**, 7749 (1991); J.D. Axe, A.H. Moudden, D. Hohlwein, D.E. Cox, K.M. Mohanty, A.R. Moodenbaugh, and Youwen Xu, Phys. Rev. Lett. **62**, 2751 (1989); B. Bchner, M. Breuer, A. Freimuth, and A.P. Kampf, J. Low Temp. Phys. **95**, 285 (1994).

[34] P. Voruganti, A. Golubentsev, and S. John, Phys. Rev. B **45**, 13 945 (1992).

[35] See, for instance, T. Timusk and B. Statt, Rep. Prog. Phys. **62**, 61 (1999).